

High-resolution Spectra of Very Low-Mass Stars[★]

C.G. Tinney^{1,2} & I.N. Reid³

¹*Anglo-Australian Observatory, PO Box 296, Epping, N.S.W. 2121, Australia. cgt@aaoepp.aao.gov.au*

²*European Southern Observatory, Garching, Germany.*

³*Palomar Observatory, 105-24, California Institute of Technology, Pasadena, CA. 91125, USA.*

Accepted —. Received —; in original form —

ABSTRACT

We present the results of high-resolution (1-0.4 Å) optical spectroscopy of a sample of very low-mass stars. These data are used to examine the kinematics of the stars at the bottom of the hydrogen-burning main sequence. No evidence is found for a significant difference between the kinematics of the stars in our sample with I–K > 3.5 ($M_{Bol} \gtrsim 12.8$) and those of more massive M-dwarfs ($M_{Bol} \approx 7 - 10$). A spectral atlas at high (0.4 Å) resolution for M8-M9+ stars is provided, and the equivalent widths of CsI, RbI and H α lines present in our spectra are examined. We analyse our data to search for the presence of rapid rotation, and find that the brown dwarf LP 944-20 is a member of the class of “inactive, rapid rotators”. Such objects seem to be common at and below the hydrogen burning main sequence. It seems that in low-mass/low-temperature dwarf objects either the mechanism which heats the chromosphere, or the mechanism which generates magnetic fields, is greatly suppressed.

Key words: stars: activity - stars: chromospheres - stars: kinematics - stars: low-mass, brown dwarfs - stars: rotation - techniques: radial velocities

1 INTRODUCTION

There have been suggestions in the recent literature of the existence of a young ($\lesssim 10^8$ yr) population of brown dwarfs in the solar neighbourhood masquerading as VLM stars. Hawkins & Bessell (1988) carried out a survey using UK Schmidt telescope plates, and claim that the reddest stars show a smaller (ie. younger) velocity dispersion than their mid-M-type stars. Kirkpatrick & McCarthy (1994) have shown that a *linear* extrapolation of their spectral-type versus mass relation implies sub-stellar masses for spectral types later than M7. In such a situation, there would be a strong bias towards detecting only young, higher-luminosity ($M_{Bol} \lesssim 13$) VLM dwarfs. More compelling, however, are the results of the CCD survey of Kirkpatrick et al. (1994) which finds a significant excess of $M_I > 12$ ($M_{Bol} \gtrsim 12$) dwarfs in the southern Galactic hemisphere: seven in 7.9 square degrees versus none within the 19.4 area surveyed at northern latitudes. Given that the Sun lies ≈ 30 pc above the Galactic mid-plane, this would be consistent with the existence of a population of very low scale-height M-dwarfs. Kirkpatrick et al. suggest that this population is young either because such low-mass stars can only form at high

metallicities, *or* because the objects are substellar, and are detected only when young. These hypotheses can be tested by estimating a kinematic age for local VLM dwarfs, and our current analysis centres on applying that test. This work supersedes the preliminary results presented by Reid, Tinney & Mould (1994 - hereafter RTM).

2 OBSERVATIONS & ANALYSIS

While proper motions are straight-forward (if tedious) to acquire for even very faint M-dwarfs, radial velocities are more difficult to measure. The low intrinsic luminosities of late-type dwarfs lead to only a relatively small number of those stars being accessible to accurate velocity measurement, particularly since those velocities should be obtained by cross-correlation on the stellar pseudo-continuum. The oft-used H α emission line is produced via chromospheric activity and may not be a reliable velocity indicator. The present sample includes 37 stars or systems bright enough in the 7000-9000 Å region ($I \lesssim 17$) to obtain radial velocities – 20 of these have $M_{Bol} \geq 12.8$.

2.1 ESO 3.6-m

Spectra were obtained using the Cassegrain Echelle Spectrograph (CASPEC) on the ESO 3.6m telescope on the nights

[★] Based on observations made at the European Southern Observatory 3.6-m telescope, La Silla, Chile, and the 5-m Hale telescope, Palomar Observatory, USA.

Table 1. Radial Velocity Measurements – Photometrically Selected Objects

Object	V_{hel}	UT	V_{mean}	I	I-K	Phot.	Posn
BRI0021-0214	$+2.6 \pm 5.0$	20 Jun 1992 12:04:48	4.3 ± 2.2	15.07	4.43	3	2
	$+12.8 \pm 4.1$	21 Jun 1992 11:56:02					
	-1.1 ± 6.5	28 Jul 1993 07:55:22					
	$+0.4 \pm 3.5$	29 Jul 1993 08:36:41					
TVLM 831-161058	$+27.0 \pm 8.8$	17 Oct 1992 09:36:55	21.2 ± 5.1	16.63	3.96	4	1
	$+32.0 \pm 11.7$	17 Oct 1992 10:12:42					
	$+13.0 \pm 7.3$	17 Oct 1992 10:40:46					
TVLM 832-10443	$+8.3 \pm 6.2$	17 Oct 1992 11:28:27	2.1 ± 5.2^c	16.06	4.07	4	1
	-13.6 ± 9.9	17 Oct 1992 12:05:06					
LP 771-21/BR 0246-1703 ^{a,b}	-25.6 ± 4.8	17 Oct 1992 08:50:09	-25.6 ± 4.8	15.42	3.95	2	2,3
LP 944-20/BRI 0337-3535 ^b	$+4.6 \pm 3.1$	28 Jul 1993 09:53:58	7.4 ± 1.3	14.16	4.58	2	2,3
	$+5.7 \pm 2.1$	29 Jul 1993 10:17:28					
	$+10.0 \pm 2.0$	09 Feb 1994 01:15:52					
BRI 1222-1222	-0.6 ± 2.0	08 Feb 1994 09:00:17	-0.6 ± 2.0	15.74	4.31	2	2,3
TVLM 513-46546	$+6.7 \pm 4.2$	19 Jun 1992 06:02:54	8.2 ± 2.2	15.09	4.32	4	1
	$+9.0 \pm 3.6$	20 Jun 1992 05:48:37					
	$+8.6 \pm 3.7$	20 Jun 1992 06:25:26					
TVLM 513-42404A ^d	-42.0 ± 6.3	21 Jun 1992 07:43:14	-40.9 ± 4.6^d	16.59	3.19	4	1
	-9.5 ± 6.5	21 Jun 1992 08:16:44					
	-39.6 ± 6.8	21 Jun 1992 08:50:48					
TVLM 513-8238	-16.8 ± 8.5	20 Jun 1992 07:56:28	-12.8 ± 3.6	17.14	4.16	4	1
	-7.1 ± 7.2	20 Jun 1992 07:22:44					
	-22.6 ± 7.8	21 Jun 1992 05:50:16					
	-21.0 ± 9.9	21 Jun 1992 06:24:37					
	-2.4 ± 7.3	21 Jun 1992 06:59:26					
TVLM 868-110639	-47.3 ± 5.3	19 Jun 1992 06:52:07	-47.3 ± 5.3	15.79	4.42	4	1
TVLM 890-60235	$+14.8 \pm 7.7$	17 Oct 1992 04:42:59	2.6 ± 3.8	16.65	3.55	4	1
	-3.3 ± 7.2	17 Oct 1992 05:20:07					
	$+6.0 \pm 8.2$	17 Oct 1992 05:58:31					
	-5.5 ± 7.5	17 Oct 1992 06:32:37					
HB 2124-4228	-5.0 ± 3.4	28 Jul 1993 05:34:31	-5.0 ± 3.4	16.29	4.11	2	4
BR 2339-0447 ^e	$+14.2 \pm 2.1$	28 Jul 1993 06:22:05	14.2 ± 2.1	11.70	3.56	3	2

NOTES:

(a) Incorrectly referred to as BRI0246-1703 by Tinney, Mould & Reid 1993. (b) These objects, though originally catalogued as proper-motion objects, were independently selected as late stars by an optical photometric survey (Kirkpatrick, Henry & Irwin 1997). They are therefore included in the “Photometric” sample. (c) A possible velocity variable, although the velocities are poor. (d) TVLM 513-42404A has a common proper motion companion with magnitude I=18.56, I-K=4.35 (Tinney et al. 1995). The measurement of -9.5 km/s was not used in calculating the mean. (e) Classified as a giant (M7-8III) by Kirkpatrick, Henry & Irwin 1997. Incorrectly referred to as BRI 2339-0447 by Tinney, Mould & Reid 1993. (f) I-K photometry is not available. A spectral type of M5.5 has been assigned by Reid, Hawley & Gizis 1995. (g) G1473 is a known binary with separation 0.2-0.8'' and P≈16 yr (Henry & McCarthy 1990). The components were not resolved by the spectrograph slit. (h) VB 8 was used as a velocity reference at ESO, so ESO observations are not included in the mean. (i) VB 10 was used as a velocity reference at Palomar, so Palomar observations are not included in the mean. (j) Optical astrometry indicates that G1831 may be an unresolved binary with a period of under two years. (Henry & McCarthy 1993 and references therein). (k) I-K photometry is not available. The spectral type is due to Kirkpatrick et al. 1991. In view of the type mismatch between the object and template, this velocity should be treated with caution. (l) GL 866AB is a known triple system, with two of the components having ~ 0.5'' separation and P=2.20 yr (Leinert et al. 1990). This probably explains the observed velocity variations. The components were not resolved by the spectrograph slit. The “mean” velocity shown should be interpreted with care in light of this.

PHOTOMETRY REFERENCES:

(1) Leggett 1992; (2) Tinney 1996; (3) Tinney, Mould & Reid 1993; (4) Kirkpatrick, Henry & Irwin 1997; (6) Hawkins & Bessell 1988; (7) Gullixson et al. 1995 and Harrington et al. 1993; (8) Weis 1988.

POSITION REFERENCES:

(1) Tinney 1993; (2) Tinney, Mould & Reid 1993; (3) Kirkpatrick, Henry & Irwin 1997; (4) Hawkins & Bessell 1988; (5) Gliese & Jahreiss 1991; (6) Luyten 1979; (7) Tinney 1996.

of 1993 July 28-29 and 1994 February 8-9 (UT). The full width at half maximum (FWHM) resolution was 16 km/s (eg. 0.43Å at 8000Å), at a dispersion of 9 km/s per pixel. The wavelength range covered was 6400Å to 9100Å, though redwards of 8045Å the wavelength coverage is not complete and suffers inter-order gaps. For the faintest stars observed at ESO ($I \lesssim 16.3$) exposures of up to 4 hours were used. Despite

the fact that the signal-to-noise in an individual pixel at this resolution is low ($S/N \approx 2.5$ at 6500Å, $S/N \approx 30$ at 9200Å), the long wavelength coverage of the instrument means that the final velocity precision is limited by the flexure, rather than S/N. Flexure is severe in CASPEC, so considerable care was taken in the observing and data reduction. Arc spectra were taken before and after each exposure, in order to provide

Table 2. Radial Velocity Measurements – Proper-motion Selected Objects

Object	V_{hel}	UT	V_{mean}	I	I-K	Phot.	Posn
LHS 2/GJ 1002	-35.7 ± 5.5	17 Oct 1992 07:32:37	-35.7 ± 5.5	10.16	2.74	1	5
LHS 112	$+14.0 \pm 4.0$	17 Oct 1992 07:53:18	14.1 ± 4.0	12.41	M5.5 ^f	8	6
ESO 207-61	$+116.6 \pm 2.1$	08 Feb 1994 02:17:06	116.4 ± 1.5	16.35	4.18	2	7
	$+116.3 \pm 2.0$	09 Feb 1994 03:04:46					
LHS 234/G1 283B	-30.8 ± 2.0	09 Feb 1994 04:25:04	-30.8 ± 2.0	12.43	3.17	1	6
LHS 248/GJ 1111	$+47.3 \pm 3.2$	17 Oct 1992 12:57:13	47.3 ± 3.2	10.53	3.27	1	5
LHS 2065	$+7.8 \pm 4.5$	17 Oct 1992 12:51:35	9.0 ± 1.8	14.44	4.46	1	6
	$+9.2 \pm 2.0$	08 Feb 1994 04:22:29					
LHS 36/G1 406	$+20.0 \pm 3.3$	21 Jun 1992 03:45:04	20.0 ± 3.3	9.39	3.31	1	5
LHS 333/G1 473AB	$+0.6 \pm 3.3$	19 Jun 1992 03:31:54	0.9 ± 1.7^g	8.92	2.86	1	5
	-2.4 ± 3.6	19 Jun 1992 03:43:00					
	$+3.6 \pm 3.5$	20 Jun 1992 03:33:03					
	$+1.8 \pm 3.4$	21 Jun 1992 03:25:15					
LHS 2351	$+2.3 \pm 2.0$	09 Feb 1994 05:44:56	2.3 ± 2.0	14.91	3.57	1	6
LHS 2397a	$+34.3 \pm 2.1$	08 Feb 1994 06:13:18	34.1 ± 1.5	15.05	4.26	2	6
	$+34.0 \pm 2.1$	09 Feb 1994 06:59:29					
LHS 2875	-44.0 ± 2.1	29 Jul 1993 23:42:57	-45.5 ± 1.4	10.58	2.05	1	6
	-46.9 ± 2.0	09 Feb 1994 07:59:21					
LHS 2876	-48.6 ± 2.0	09 Feb 1994 08:40:30	-48.6 ± 2.0	15.76	3.59	2	6
LHS 2924	-32.5 ± 4.5	19 Jun 1992 05:23:58	-33.4 ± 2.9	15.21	4.54	1	6
	-34.0 ± 3.7	21 Jun 1992 05:06:08					
LHS 2930	-10.7 ± 3.3	20 Jun 1992 04:31:55	-10.7 ± 3.3	13.31	3.59	1	6
LHS 3003	$+1.9 \pm 2.0$	09 Feb 1994 07:35:41	1.9 ± 2.0	12.66	3.66	2	6
LHS 427/G1 643	$+22.3 \pm 5.7$	17 Oct 1992 02:16:59	17.4 ± 1.4	9.04	2.30	1	5
	$+15.3 \pm 2.0$	28 Jul 1993 02:50:07					
	$+18.8 \pm 2.0$	08 Feb 1994 09:37:38					
LHS 428/G1 644AB	$+20.2 \pm 6.2$	17 Oct 1992 02:10:56	19.3 ± 1.6	6.55	2.16	1	5
	$+19.4 \pm 3.2$	28 Jul 1993 03:04:22					
	$+19.2 \pm 2.0$	08 Feb 1994 09:42:51					
LHS 429/G1 644C/VB 8	$+15.7 \pm 3.7$	17 Oct 1992 02:35:48	16.1 ± 1.4^h	12.24	3.42	1	5
	$+16.4 \pm 3.1$	19 Jun 1992 06:57:54					
	$+15.2 \pm 3.2$	19 Jun 1992 08:38:31					
	$+17.5 \pm 3.3$	20 Jun 1992 06:33:39					
	$+15.8 \pm 3.3$	21 Jun 1992 09:01:32					
	$+13.3 \pm 2.1$	29 Jul 1993 02:24:31					
	$+14.4 \pm 2.0$	09 Feb 1994 09:31:43					
LHS 57/G1 699	-112.3 ± 5.1	19 Jun 1992 08:40:35	-112.3 ± 5.1	6.77	2.25	1	5
LHS 474/G1 752B/VB 10	$+34.8 \pm 3.1$	20 Jun 1992 09:27:42	35.3 ± 1.5^i	12.80	3.98	1	5
	$+34.9 \pm 2.1$	28 Jul 1993 03:32:50					
	$+35.7 \pm 2.1$	29 Jul 1993 04:25:38					
LHS 511/G1 831	-56.5 ± 2.0	28 Jul 1993 05:47:10	-56.5 ± 2.0^j	9.02	2.60	1	5
LHS 515	$+59.5 \pm 7.7$	17 Oct 1992 03:33:19	59.5 ± 7.7	15.16	sdM2.5 ^k		6
LHS 523	-7.4 ± 3.9	17 Oct 1992 03:48:55	-7.4 ± 3.9	13.00	3.10	1	6
LHS 68/G1 866AB	-43.2 ± 3.7	19 Jun 1992 11:18:37	-49.6 ± 2.8^j	8.62	3.06	1	5
	-58.2 ± 4.3	21 Jun 1992 11:54:01					

NOTES, PHOTOMETRY and POSITION REFERENCES: See Table 1.

a mean wavelength zero-point. The instrumental velocity system so constructed was checked by cross-correlating the wavelength calibrated night-sky spectra against each other – from which we derive a systematic uncertainty due to flexure of 2 km/s.

The radial velocity system was calibrated initially using observations of the preliminary IAU M-giant standard α Cet ($V_{hel} = -25.8 \pm 0.5$ km/s; Trans.IAU,XXIB,275). By cross-correlation with α Cet we determined the heliocentric radial velocity of VB 8 to be 14.5 ± 1.0 km/s and of VB 10 to be 34.4 ± 1.3 km/s. VB 8 was then adopted as the cross-correlation template for *all of the CASPEC data*, with an assumed $V_{hel} = 14.5$ km/s. Cross-correlations were carried

out on an order-by-order basis, using regions of the spectrum free of atmospheric absorption and strong sky lines. The results for each order were then combined as a weighted mean to produce a velocity shift for each exposure. Tables 1 and 2 show measured radial velocities for each observation. The uncertainties quoted for individual observations are based on the uncertainty produced by the cross-correlation procedure of Tonry & Davis (1979)[†], combined with the systematic

[†] RTM used an empirical technique to estimate cross-correlation velocity uncertainties, together with the expressions of Tonry & Davis (1979). Based on this it was stated that the Tonry & Davis

2 km/s uncertainty due to spectrograph flexure – for most targets it is this systematic uncertainty which dominates.

2.2 Palomar 5-m

Radial velocities were obtained using the red arm of the Double Spectrograph on the Hale 5m telescope, on 1992 June 19-22 (UT) and 1992 October 16-17 (UT). A 1200 line/mm grating was used in the following configurations: 76 km/s (2.15Å) resolution at a dispersion of 28 km/s (0.80Å) per pixel, over 8110-8735Å in June 1992; and 74 km/s (1.78Å) resolution at a dispersion of 36 km/s (0.81Å) per pixel over 7906–7549Å. These are the same observations reported by RTM. However, in the course of checking our CASPEC radial velocities against both the literature and the results of RTM, it became clear that there were problems with the RTM velocities, which at that time could not be checked against other observations owing to a lack of published velocities for late M-dwarfs.

We have re-reduced the RTM data, taking the care to ensure a rigid velocity system with the CASPEC data. Calibration arcs show flexure in the Double Spectrograph of up to 20 km/s over the course of a night, so arcs were taken before and after each exposure of longer than 15 minutes. Cross correlations of arcs before and after long exposures reveal no flexure larger than 5 km/s. We adopt a lower limit to the precision of our velocities of 3 km/s based on our ability to calibrate out this flexure.

VB 10 was adopted as the velocity template, with an assumed $V_{hel} = 35$ km/s (based on our CASPEC observations). VB 10 was adopted in preference to VB 8, as it was felt that at the lower spectral resolution of the Palomar data a good spectral-type match between template and object is more important. The results of this re-reduction are also shown in Tables 1 and 2.

2.3 Combined Results

The final velocities are weighted means of the individual observations. Amongst the current sample, only G1866AB shows compelling evidence for velocity variability. The velocity difference seen in exposures separated by only 2 days is 15.0 ± 5.7 km/s. G1866AB has been resolved by infrared speckle techniques as a binary system with period of 2.2 years and separation of between 0.2-0.8'' by Leinert et al. (1990). However, Leinert et al. (1997) report a private communication from A.Duquennoy & D.Latham to the effect that a third component has been detected spectroscopically. Reid & Gizis (1997) also report the detection of an SB2 component, with a period inconsistent with that of the resolved components. Our current results add further support for the presence of a third component in this system.

TVLM 832-10443 and TVLM 513-42404A both show possible evidence for velocity variability, although the data are of poor quality. In the case of TVLM 513-42404A where

algorithm gave systematically low uncertainties. It is now known that this was due to an error in our implementation of their algorithm – the correct algorithm gives similar uncertainties to our empirical technique.

Table 3. Radial velocities compared with other studies.

Object	V_{hel} Literature	V_{hel} This work	ΔV_{hel}
Marcy & Benitz (1989)			
G1 699	-110.9±0.2	-112.3±5.1	1.4±5.1
G1 831	-57.1±1.0	-56.5±2.0	-0.6±2.2
Delfosse, Forveille, Perrier & Mayor (1998)			
GJ 1002	-41±1	-35.7±5.5	-5.3±5.1
GJ 1111	9±1	47.3±3.2	-38±3.3
G1 406 ^a	19.2±0.2	20.0±3.3	-0.8±3.3
G1 699	-111±1	-112.3±5.1	-1.3±5.2
Basri & Marcy (1995)			
GJ 1111	11.4±3 ^b	47.3±3.2	-36±4
BRI 0021-0214	15.6±3 ^b	4.3±2.2	11.3±3.7

NOTES:

a – G1406 velocity is not that from Table 2 of Delfosse et al., but the more precise value quoted in Martín et al. 1997. *b* – Basri & Marcy used G1406 as a velocity standard with an assumed velocity of 16.5 km/s. The velocities they give have been corrected to using more precise velocity for G1406 given by Delfosse et al. 1998.

three observations are available, we have rejected the discrepant value to estimate a mean velocity. For TVLM 832-10443 we use the mean of the two available velocities.

In Table 3 we compare the velocities derived in this study with those obtained by other studies – in particular those of Marcy & Benitz (1989), Delfosse et al. (1998) and Basri & Marcy (1995). An examination of this table shows that with only two exceptions our velocities are all consistent within 1- σ uncertainties with those obtained from the literature.

Those exceptions are GJ 1111 and BRI 0021-0214. In the case of GJ 1111 we can find no plausible explanation for the velocity difference observed. The remote possibility that GJ 1111 is a radial velocity variable is argued against by the consistent velocities for it determined at several epochs over the last 2 years at Observatoire de Haute Provence (X.Delfosse, priv.comm.). The target observed and the data reduction for this object have been thoroughly checked. We can find no fault to which this discrepancy (which corresponds to approximately one pixel on our detector) can be adduced. The observations of LHS 2065, VB 8 and G1643 made on the same night as GJ 1111, show that the velocity system for this night was consistent with that obtained on all other observing runs.

Our velocities for BRI 0021-0214 show marginal evidence for variability. Moreover, they are also significantly different from that obtained by Basri & Marcy in November 1993. Multiple observations on that run ruled out velocity variability on 90 minute timescales at the 3 km/s level (indicating the “system” is not a close, tidally-locked binary). The two combined sets of data therefore suggest $\sim 2 - 12$ month velocity variability at the 10 km/s level. Further observations are required to confirm or reject this hypothesis. It should also be noted that both we (§6) and Basri & Marcy find BRI 0021-0214 to be a rapid rotator ($v \sin i \approx 40$ km/s). This means its cross-correlation peak is significantly broad-

Table 4. Derived Velocities

Object	V_{tan} km/s	U^a km/s	V^a km/s	W^a km/s	V_{total}^b km/s	Sample ^c	Astrometry References
BRI 0021-0214	8.5± 0.5	-8.8± 0.5	-3.2± 1.5	-2.6± 2.6	9.7± 3.0	A	1
TVLM 831-161058	63.6± 8.2	-65.5± 6.0	-43.2± 4.6	10.6± 5.9	79.1± 9.6	A	1
TVLM 832-10443	26.3± 2.4	9.5± 3.4	-5.4± 2.8	-23.9± 3.6	26.3± 5.7	A	1
LP 771-21/BR 0246-1703	21.8± 2.2	16.1± 3.0	-24.0± 2.9	12.3± 3.2	31.4± 5.3	A	2
LP 944-20/BRI 0337-3535	10.3± 0.3	-20.6± 0.8	-15.9± 0.8	-7.3± 0.7	27.1± 1.3	A	2
BRI 1222-1222	26.0± 1.9	-20.8± 1.4	-30.8± 1.5	-18.2± 1.8	41.3± 2.8	A	2
TVLM 513-46546	4.0± 0.4	-4.0± 1.3	-12.5± 1.2	1.5± 1.4	13.2± 2.2	A	1
TVLM 513-42404A	17.2± 5.1	-30.6± 3.9	-37.6± 3.4	-34.2± 4.0	59.3± 6.8		1
TVLM 513-8238	24.2± 4.8	-19.6± 3.4	-36.2± 3.0	-6.5± 3.5	41.7± 6.0	A	1
TVLM 868-110639	31.4± 2.6	-60.3± 3.7	-28.7± 2.8	-22.8± 3.6	70.5± 5.9	A	1
TVLM 890-60235	17.7± 2.0	7.9± 2.1	-8.8± 2.1	-0.5± 3.1	11.8± 4.3	A	1
HB 2124-4228	72.2±15.5	-17.7± 8.1	-82.8±10.0	-6.5± 9.1	84.9±15.8	A	1
LHS 2/GJ 1002	45.5± 0.8	27.9± 0.7	-49.6± 2.8	16.1± 4.8	59.2± 5.6		2
LHS 112	81.5± 4.0	-52.0± 2.7	-50.1± 3.1	-64.8± 3.5	97.0± 5.7		4
ESO 207-61	34.3± 2.9	-61.0± 2.3	-118.1± 2.0	-29.4± 1.3	136.1± 3.3	B	2
LHS 234/GI 283B	53.0± 2.5	45.7± 1.8	-10.6± 1.6	21.6± 1.9	51.7± 3.2		4
LHS 248/GJ 1111	22.2± 0.4	-57.0± 2.1	-30.3± 1.7	0.9± 1.7	64.6± 3.2		4
LHS 2065	22.0± 0.3	-23.1± 1.2	-22.1± 0.9	-21.6± 1.1	38.6± 1.8	B	3
LHS 36/GI 406	53.1± 0.3	-36.9± 0.9	-58.8± 1.6	-18.9± 2.7	71.9± 3.3		4
LHS 333/GI 473AB	37.4± 0.7	-43.0± 0.7	-26.4± 0.9	-6.2± 1.5	50.9± 1.9		4
LHS 2351	49.0± 4.3	-54.8± 2.9	6.2± 2.9	-2.0± 2.4	55.2± 4.8	B	4
LHS 2397a	38.3± 2.5	-39.0± 2.1	-51.7± 1.3	2.6± 1.4	64.8± 2.9	B	3
LHS 2875	102.6±12.6	-116.5± 9.0	-41.9± 6.3	2.3± 6.3	123.9±12.7		2
LHS 2876	102.6±12.6	-118.2± 9.0	-41.3± 6.3	-0.2± 6.4	125.2±12.8	B	2
LHS 2924	40.0± 0.6	-1.8± 1.5	-57.5± 1.7	-28.4± 1.9	64.2± 3.0	B	3
LHS 2930	37.1± 0.5	-37.0± 1.6	-37.5± 2.3	-4.4± 1.8	52.9± 3.3	B	3
LHS 3003	28.8± 1.0	-12.6± 1.3	-37.1± 1.3	-17.7± 1.3	43.0± 2.2	B	2
LHS 427/GI 643	32.7± 1.3	11.6± 1.3	-39.8± 1.0	4.8± 0.9	41.7± 1.9		4
LHS 428/GI 644AB	36.2± 0.6	13.9± 1.4	-42.9± 0.8	6.0± 0.6	45.5± 1.7		4
LHS 429/GI 644C/VB 8	36.0± 0.6	9.4± 1.7	-43.6± 1.0	4.4± 0.7	44.8± 2.1		3
LHS 57/GI 699	89.4± 0.2	-151.3± 4.4	-7.2± 2.3	11.9± 1.0	152.0± 5.1		4
LHS 474/GI 752B/VB 10	42.4± 1.8	44.9± 1.8	-20.3± 1.5	-11.8± 1.1	50.6± 2.7	B	1,2,3
LHS 511/GI 831	45.1± 1.8	-73.3± 1.6	-43.6± 1.3	-0.7± 1.7	85.3± 2.7		4
LHS 515	267.9±55.0	-107.2±37.2	-126.1±29.8	-234.9±26.7	287.4±55.5		4
LHS 523	55.9± 3.4	22.8± 2.2	-57.5± 3.1	-6.6± 3.5	62.2± 5.2		4
LHS 68/GI 866AB	52.6± 0.6	-73.9± 1.0	-8.1± 1.5	25.8± 2.2	78.7± 2.9		4

NOTES:

a – Note that the uncertainty ellipse associated with the *measured* space velocities does not have axes orthogonal to the (U,V,W) co-ordinate system. This means that the uncertainties in the U,V,W velocities are not independent, and so they do not add in quadrature to give the uncertainty in the total space velocity.

b – Magnitude of the total space velocity, corrected for the basic solar motion as described in the text.

c – **Sample A** is the set of photometrically selected objects with $I-K > 3.5$ (ie $M_{Bol} > 12.8$). It also includes the binary companion TVLM 513-42404B, which is assumed to have the same radial velocity, distance and proper motion as TVLM 513-42404A. **Sample B** is the set of proper motion selected objects with $I-K > 3.5$ (ie $M_{Bol} > 12.8$).

ASTROMETRY REFERENCES:

(1) Tinney et al. 1995; (2) Tinney 1996; (3) Monet et al. 1992; (4) van Altena, Lee & Hoffleit 1995.

ened, making it possible that the velocity variability observed is simply due to the uncertainty in measuring the centroid of a broadened peak.

With the exception of these two objects, our velocities are consistent with external observations and we conclude that they are accurate to the stated precisions. In particular, we are now confident that our re-reduction of the Palomar radial velocity data provides a robust velocity system, consistent with our ESO data and with independent observations. *The data presented in Tables 1 and 2, therefore, supersede that presented in RTM, which should no longer be used.*

3 RADIAL VELOCITIES & SPACE VELOCITIES

The current sample includes 37 stars; 20 fainter than $M_{Bol} = 12.8$ ($I-K > 3.5$) and 17 brighter (the two stars with no $I-K$ colour data are clearly more luminous than $M_{Bol} = 12.8$, given their a spectral types of M5.5V and sdM2). A subset of these stars were identified originally through their substantial proper motions, and one might expect that subset to be biased toward higher velocities. To take this into account, we define two sub-samples:

Sample A - is the set of photometrically selected objects with $I-K > 3.5$ ($M_{Bol} > 12.8$), containing 12 objects (Table 1);

Table 5. Mean Velocities and Dispersions for VLM Stars.

	Weighted			Unweighted		Early M dwarfs	
	Sample A	Sample B	Sample A+B	Sample A	Sample B	Sample A+B	
	(km/s)	(km/s)	(km/s)	(km/s)	(km/s)	(km/s)	
$\langle U \rangle$	-13±7	-34±14	-17±8	-18±7	-34±14	-25±7	-18.6
$\langle V \rangle$	-20±6	-42±11	-30±6	-27±6	-42±11	-33±6	-32.1
$\langle W \rangle$	-8±4	-13±4	-10±3	-8±4	-13±4	-10±3	-13.6
σ_U	18	34	26	25	45	35	38.2
σ_V	16	30	25	22	34	28	25.7
σ_W	23	30	25	25	34	27	20.5

NOTES:

a - The “Complete” sample results from Table 9 of HGR, but corrected for basic solar motion as for our data (§3).

Sample B - is the set of proper motion selected objects with $I-K > 3.5$ ($M_{Bol} > 12.8$), containing 9 objects (Table 2).

Table 4 lists the Galactic (U,V,W) space motions (U positive toward the Galactic Centre), where we correct for a Basic Solar Motion of (9,11,6) km/s (Mihalas & Binney 1981). In each case, the radial velocity and proper motion uncertainties were propagated into the (U,V,W) system. However, it should be noted that since the uncertainties in U,V and W are not independent, they do not add in quadrature to give the uncertainty in the total space velocity.

None of the “confirmed” radial velocity variables in Tables 1 and 2 (eg. G1866AB) are included in Samples A or B. The possible variables BRI 0021-0214 and TVLM 832-10443 are included pending a final determination of their status – in any case their velocity variation is of the order of the quoted uncertainty in their velocities. The total number of objects in Samples A and B is only slightly larger than that used in the equivalent samples of RTM (ie 21 versus 18), but the precision is improved significantly and none of the current radial velocities are derived from H α emission. Altogether, the conclusions we derive from these new data can be expected to be considerably more robust.

Table 5 shows the means ($\langle U \rangle, \langle V \rangle, \langle W \rangle$) and standard deviations ($\sigma_U, \sigma_V, \sigma_W$) of the Galactic velocity distributions for Samples A, B and A+B. Both weighted and unweighted estimates of these quantities are shown. The same quantities are shown for the 346 stars of the more luminous ($M_V \approx 8 - 13$, or $M_{Bol} \approx 7.4 - 10.4$) volume-complete sample of Hawley, Gizis & Reid (1997 - hereafter HGR), with the same correction applied for basic solar motion. Figures 1-3 show the V_{total} , U, V, and W velocity distributions for the same three samples, together with the corresponding distributions from HGR.

Inspection of Table 5 shows that whether weighting is used or not makes no significant difference to the observed means – which are in all cases consistent with those observed for the more massive stars of HGR. The value of the velocity dispersion depends slightly on whether weighting is used, with the weighted values being somewhat smaller. Again, however, there is no indication in any case that the velocity dispersion for VLM stars is smaller than that seen for early M-dwarfs.

Table 6. K-S Test Results – the probabilities, for each velocity component, that the hypotheses described in the text are true.

	Hypothesis			
	(a)	(b)	(c)	(d)
Velocity				
U	33%	78%	67%	53%
V	33%	89%	77%	32%
W	96%	17%	12%	91%

Because such an “eyeball” comparison can be misleading, we have performed Kolmogorov-Smirnov tests (see eg. Press *et al.* 1986) to test the following hypotheses:

- (a) that Samples A and B are drawn from the same statistical population;
- (b) that Sample A+B is drawn from the same statistical population as the HGR sample;
- (c) that Sample A is drawn from the same statistical population as the HGR sample;
- (d) that Sample B is drawn from the same statistical population as the HGR sample;

The results of these tests are shown in Table 6 and provide no evidence that samples A and B are drawn from different parent populations. Figs 1-3 suggest possible kinematic differences between the VLM-dwarf and HGR samples. However, the K-S tests show that all of the samples are indistinguishable statistically.

4 A SPECTRAL ATLAS AT 0.43Å RESOLUTION

High resolution echelle spectrographs efficient enough to observe faint targets have been used now for several years to study the lowest mass stars (eg. Basri & Marcy 1995; Schweitzer *et al.* 1996). Despite this the available atlases for these objects are all based on data taken at low resolution (eg. Kirkpatrick *et al.* 1991, 18Å; Turnshek *et al.* 1985, 8-12Å). We therefore present in Figures 4-9 an atlas showing CASPEC spectra of three objects; the M7 dwarf VB 8 (Kirkpatrick *et al.* 1991); the M9 dwarf LHS 2065 (Kirkpatrick *et al.* 1991) and the >M9V brown dwarf LP 944-20 (Kirkpatrick *et al.* 1997; Tinney 1998).

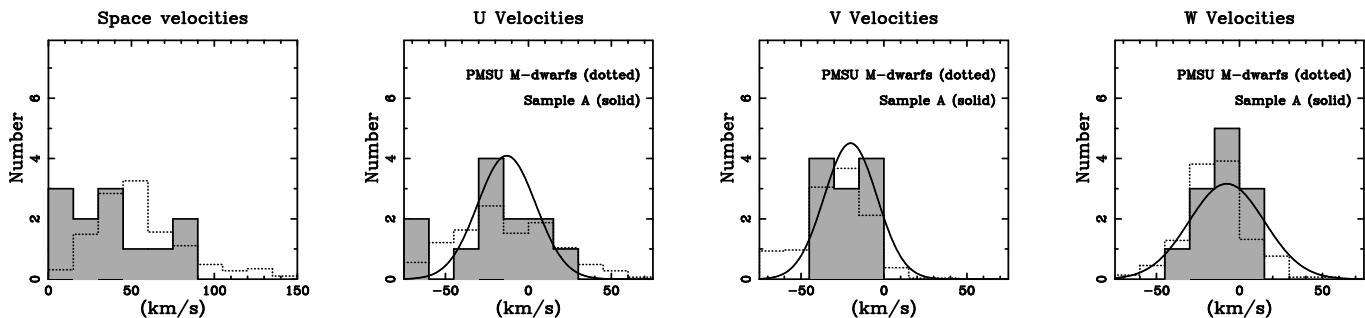


Figure 1. The V_{total} , U, V and W velocity distributions for Sample A are shown as shaded. A solid Gaussian shows the weighted mean and dispersion. The dotted histogram is the “Complete” sample of HGR, normalised to the same total counts as Sample A. All velocities have been corrected for the basic solar motion as described in the text.

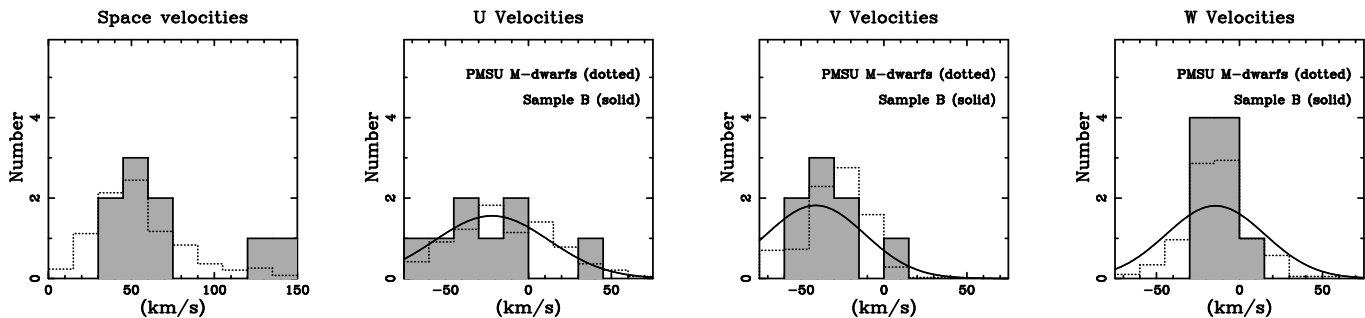


Figure 2. As for Fig. 1, but for Sample B.

These spectra have been flux calibrated using observations of the standard star μ Columbae (Turnshek et al. 1990). Because our observations were not made with a spectrophotometric slit, we only obtain a relative inter-order calibration. An absolute calibration has been obtained by scaling to the published I-band photometry of these objects (Leggett 1992) using a zero-magnitude flux of 2550 Jy (Reid & Gilmore 1984). The overall flux calibration is accurate to $\pm 10\%$ – however the inter-order calibration is much better and good to a few percent. Photon counting errors were carried throughout the reduction. The signal-to-noise ratio (SNR) as a function of wavelength for our spectra is summarised in Fig 10. Digital copies of the atlas spectra (including the SNR spectra) have been deposited with the NASA Astrophysics Data Centre.

4.1 Terrestrial Features

The spectra shown have not been corrected for terrestrial absorption due to O_3 and H_2O (cf. Allen 1976, §58 and references therein). The locations of terrestrial absorption in these spectra can be seen in the panel showing the normalised flux from the standard star μ Col. The effects of O_3 are quite regular and straightforward to disentangle from features in the stars themselves. This is not true for H_2O absorption which is complex and irregular. We therefore show in the stellar panels the locations of the strongest lines of H_2O absorption. Also shown are the locations of the stellar absorptions present in μ Col itself.

4.2 Molecular Features

The dominant molecular features in these spectra are due to TiO and VO. The figure shows the locations of identified bandheads due to these two species. Also shown are the spectroscopic “systems” to which these bandheads have been assigned. Information on the actual state transitions to which these systems correspond can be found in the references provided below – in particular see Pearse & Gaydon (1976). It is important to emphasise that these identifications represent only the bandheads – more widely spread transitions cover almost all of the optical and infra-red spectra of these stars. Between 8700Å and 8850Å for example there are no major bandheads, but the spectra clearly contain numerous molecular features, as can be seen in the laboratory spectra of Gatterer et al. (1957).

4.2.1 TiO

All the TiO bandheads are observed to be degraded to the red. Where no reference is given consult Pearse & Gaydon (1976), Solf (1978), Gatterer et al. (1957) and Turnshek et al. (1985). Indicated are: the γ or “Red” system bandheads at 6651.5, 6681.1, 6714.4, 6719.3, 6746.7, 6781.3, 6814.7, 6849.9, 6852.3, 6883.6, 6918.9, 7054.5, 7059.2, 7087.9, 7093.1, 7124.9, 7125.6, 7130.4, 7159.0, 7197.7, 7219.4, 7230.8, 7269.0, 7589.6, 7628.1, 7666.4, 7672.1, 7705.2, 7742.8, 7751.6, 7782.7, 7820.1, 7828.0, 7861.0, 7881.2, 7907.3, 7948.6, 8205.8, 8250.6, 8289.0, 8302.9, 8334.5, 8375.5, 8386.5, 8419.5, 8442.3, 8451.7, 8457.1, 8471.6, 8505.5, 8513.1, 8558.4, 8569.4, and 8645.5Å; the γ' or “Orange-Red” system bandheads at 6569.3, 6596.2 and

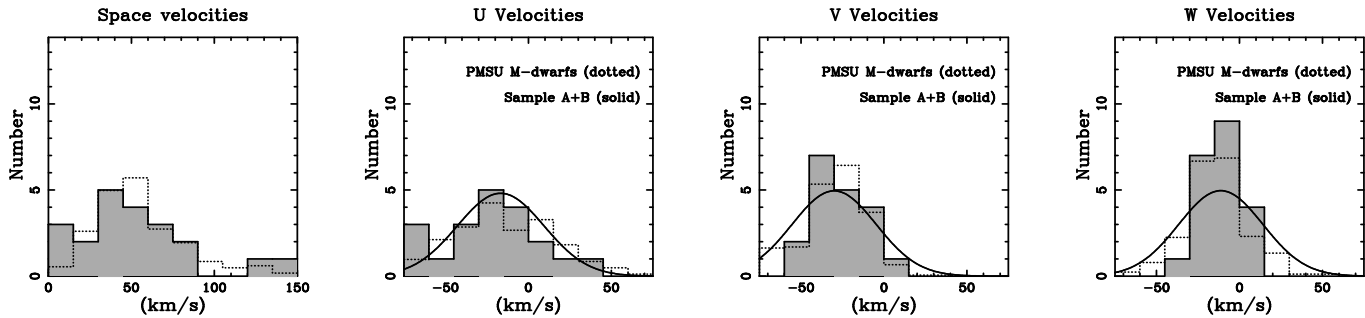


Figure 3. As for Fig. 1, but for Sample A+B.

6629.0Å; an unnamed system with bandheads at 8432, 8442 and 8452Å (Solf 1978); and an “Infrared” system with bandheads at 8859.6, 8868.5, 8937.4, 8949.8, 9014.6 and 9094.5Å (Philips 1950). Also shown is a bandhead which fits into no system at 8198.5Å (Solf 1978)

4.2.2 VO

Unlike TiO which produces distinctive bandheads degraded to the red, VO in M-dwarfs produces more diffuse absorption. Where no reference is given consult Pearse & Gaydon (1976), Solf (1978), Gatterer et al. (1957) and Turnshek et al. (1985). Indicated are: the B or “Red” system bandheads at 6876.2, 6894.0, 6919.0, 6951.6, 7011.0, 7070.2, 7131.7, 7418.2, and 8642.1Å; the C or “Infrared” system bandheads at 7333.8, 7345.3, 7372.4, 7374.8, 7393.2, 7405.2, 7433.6, 7435.3, 7444.0, 7454.0, 7466.0, 7472.1, 7492.0, 7534.1, 7850.9, 7865.0, 7896.0, 7899.6, 7918.4, 7928.5, 7938.9, 7947.7, 7960.1, 7967.2, 7973.1, 7982.1, 8520.9, 8537.7, 8572.8, 8575.3, 8590.7, 8597.2, 8604.0, 8624.0, 8648.6, 8657.9 and 8666.6Å.

4.2.3 FeH

FeH bandheads are seen degraded to the red. Indicated are the $^4\Delta$ - $^4\Delta$ system bandheads at 7786, 8692 and 9020Å (Philips et al. 1987).

4.3 Atomic Features

Atomic features shown are: H α 6562.8Å; LiI 6708.0Å; KI 7664.9Å and 7699.0Å; RbI 7800.2Å and 7947.6Å; NaI 8183.3Å and 8194.8Å; CsI 8521.4Å and 8943.6Å; BaI 7911.3Å. With the exception of H α all these lines are resonance transitions. The weak lines of CaII, MgI and TiI seen in earlier M-dwarfs (Kirkpatrick et al. 1991) are undetectable amongst the morass of molecular absorptions in these M7-M9+ dwarfs. The LiI detection seen in LP 944-20 in Fig. 4 is discussed in Tinney (1998).

It is particularly interesting to note the pronounced width of the KI lines in VB 10 compared with the two cooler objects. Schweitzer et al. (1996) have modelled the atomic lines of VB10, and find that this extreme strength of KI could be due to either high metallicity ($[M/H]=+0.5$) or high gravity ($\log g=5.5$). Schweitzer et al. did not explore the temperature dependence of KI line strength, however the spectra shown in Fig. 6 would seem to imply that either

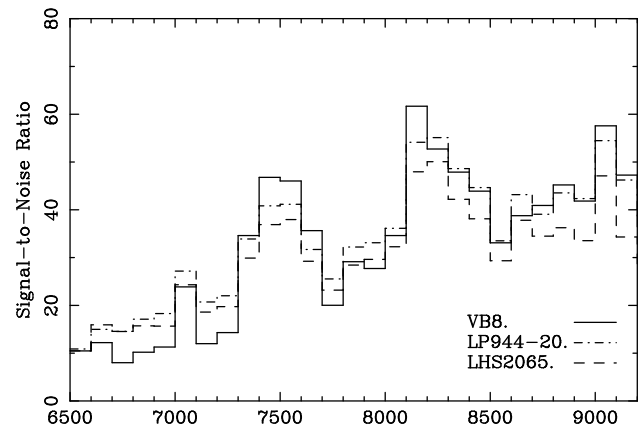


Figure 10. Signal-to-noise ratios as a function of wavelength for the spectra shown in Figs 4-9.

KI weakens slightly with decreasing effective temperature, or that VB 10 has an unusually high metallicity or gravity.

5 SPECTRAL FEATURES

5.1 Atomic Lines

In this section we deal only with the high resolution observations made at La Silla. Na I and KI lines are prominent in almost all of these spectra, however measurement of them is made difficult by the presence of atmospheric absorption, which we did correct for this study.

Cs I and Rb I lines, however, lie in regions of the spectrum clear of atmospheric absorption, and become prominent for late-type dwarfs (Tinney 1997). The measured equivalent widths of these lines are shown in Table 7. Because no part of the spectrum is free of stellar molecular absorption, the assignment of a true continuum is impossible. As a result whenever we refer to equivalent widths, they are always defined relative to the apparent continua available near the lines. The uncertainties presented in the table are based on photon-counting errors and do not include systematics due to pseudo-continuum placement. However, our measurements should be self-consistent within this set of observations and with other observations obtained at similar resolution. We have also included results from Martín et al. 1997 for two cool objects discovered in the DENIS survey (Delfosse et al. 1997; Tinney, Delfosse & Forveille 1997).

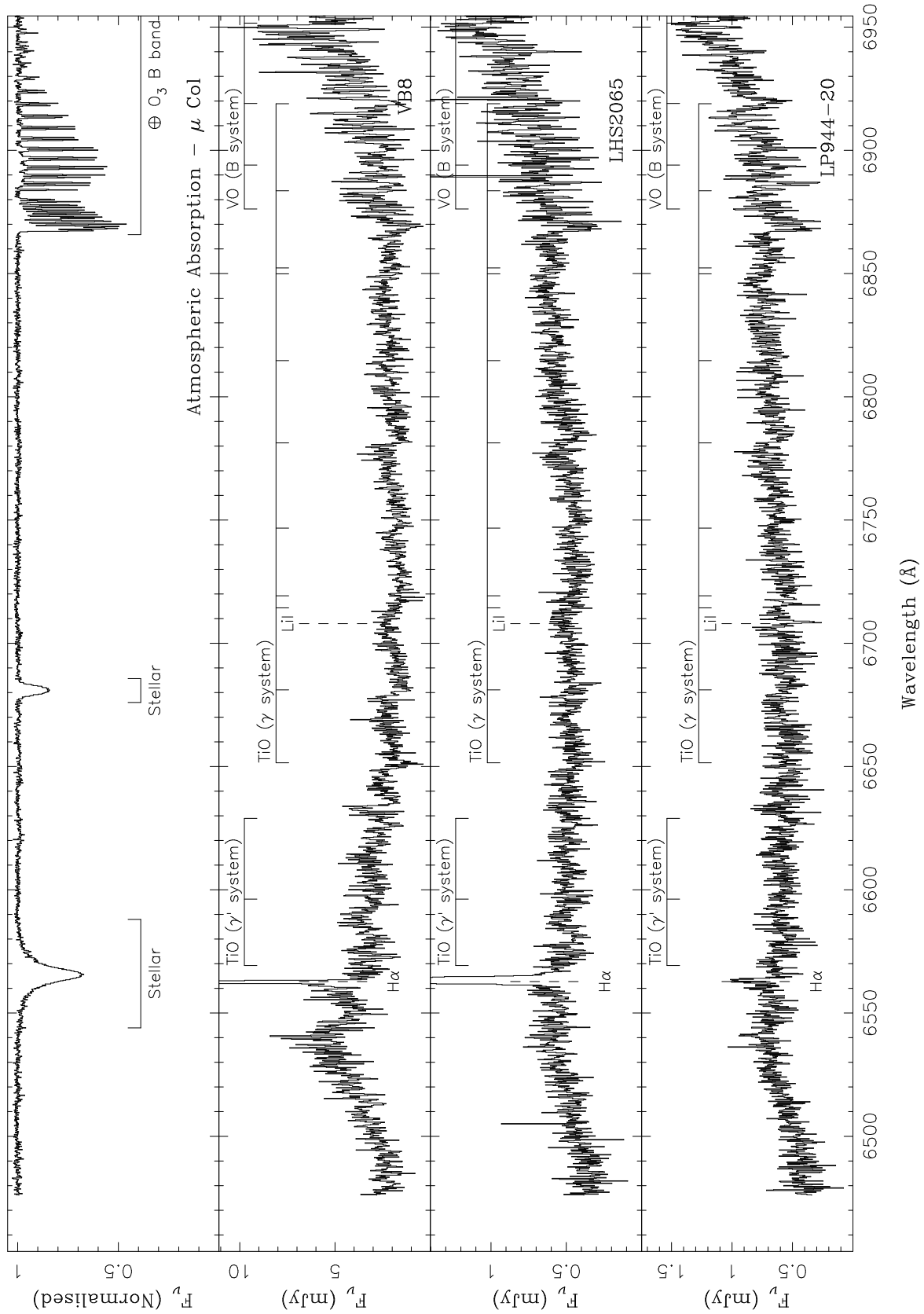


Figure 4. A spectral atlas for the objects VB 8, LHS 2065, and LP 944-20 at 0.43 Å resolution. The normalised spectrum of the standard star μ Col shows the location of terrestrial atmospheric features. The bottom of the scale in each panel is 0.0.

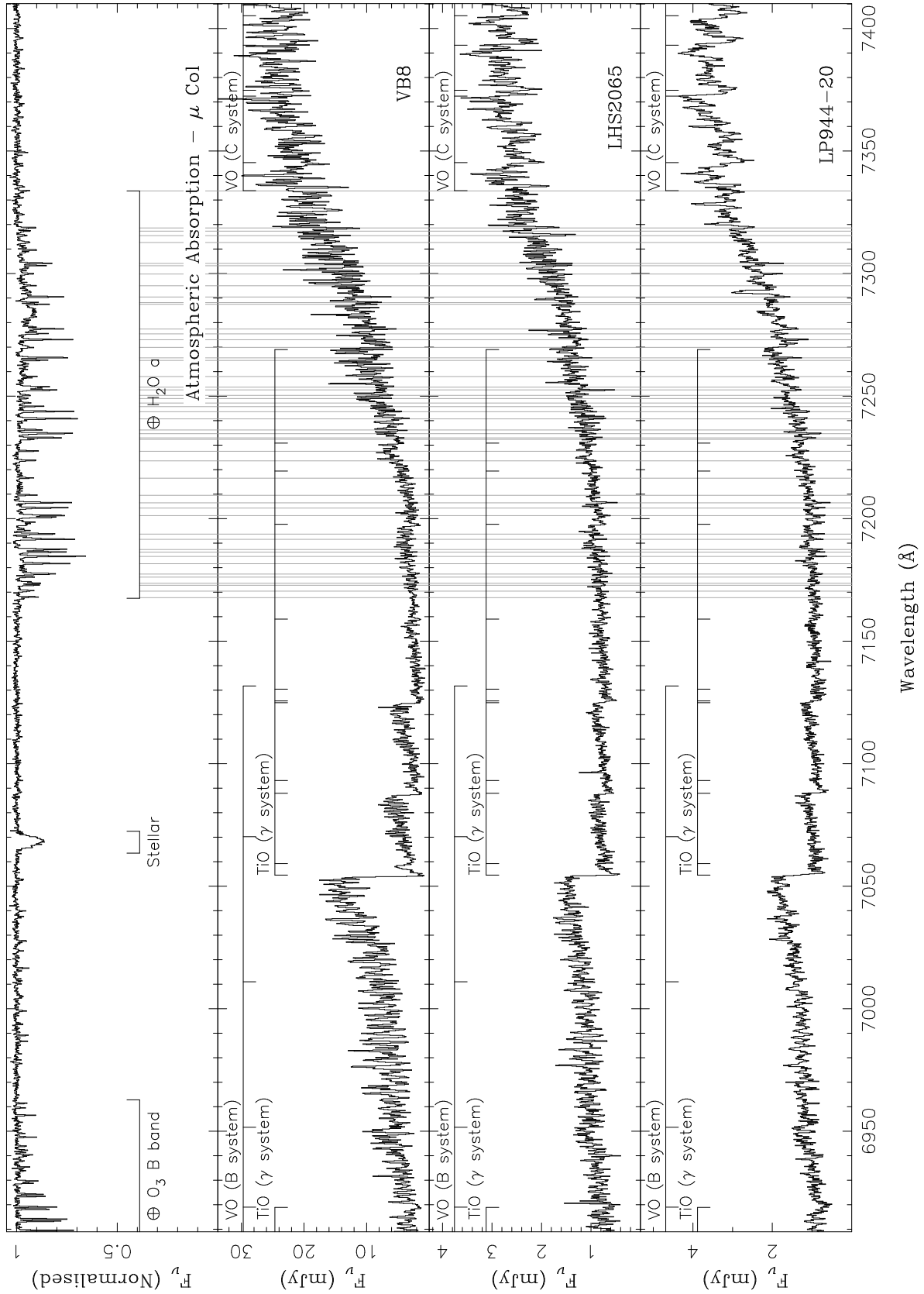


Figure 5. A spectral atlas for the objects VB8, LHS 2065, and LP 944-20 at 0.43 \AA resolution (continued).

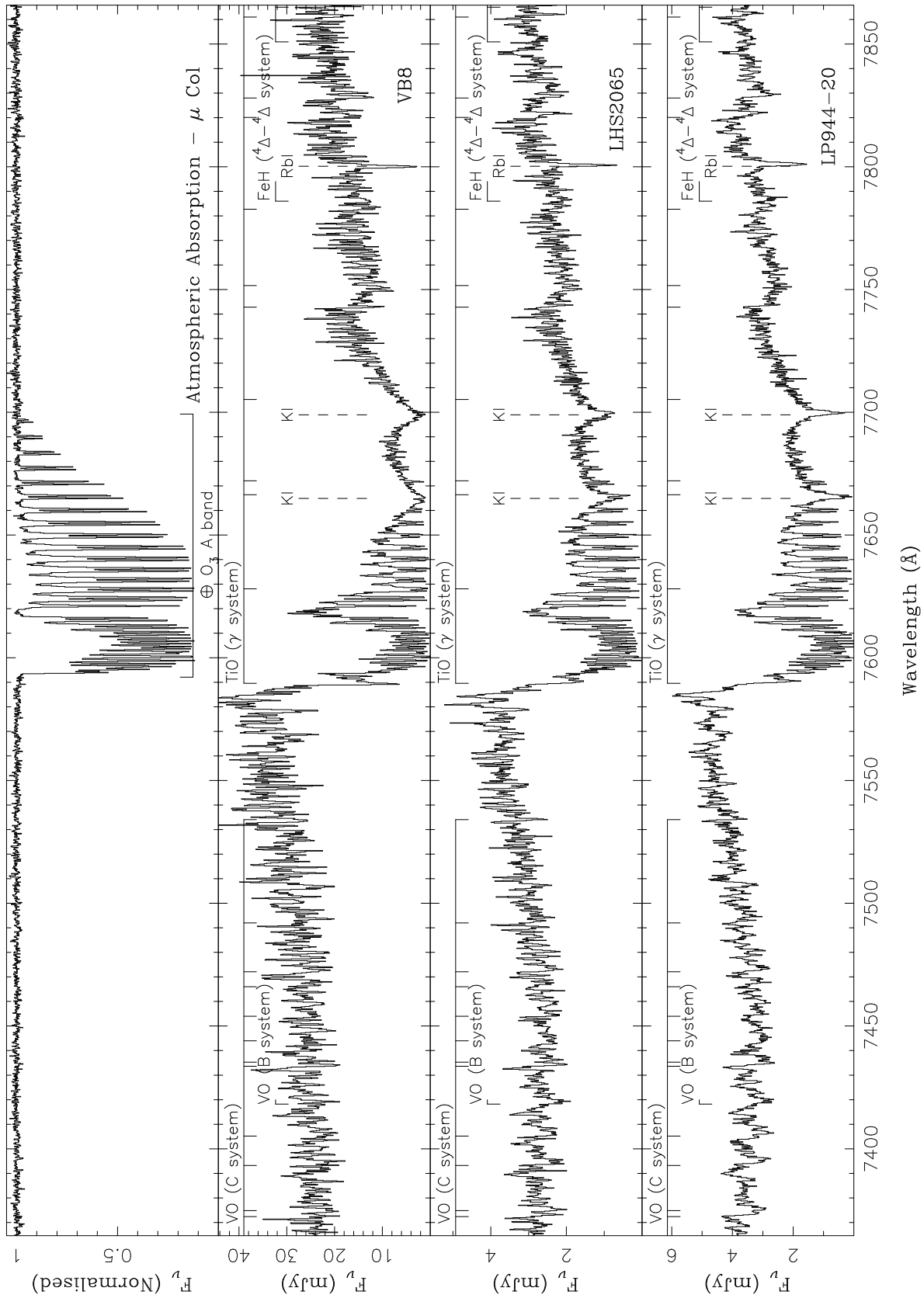


Figure 6. A spectral atlas for the objects VB8, LHS2065, and LP944-20 at 0.43\AA resolution (continued).

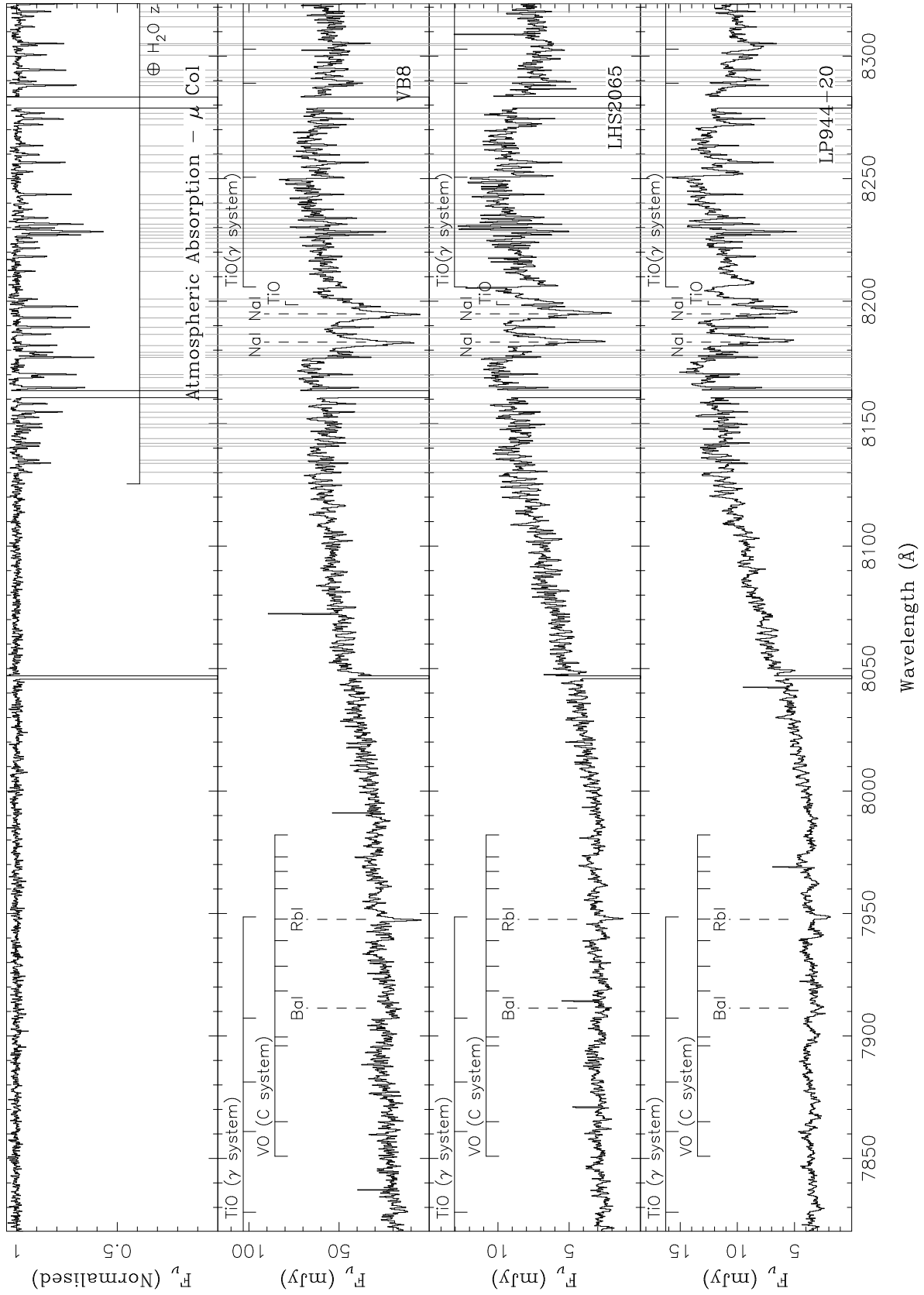


Figure 7. A spectral atlas for the objects VB8, LHS2065, and LP944-20 at 0.43\AA resolution (continued).

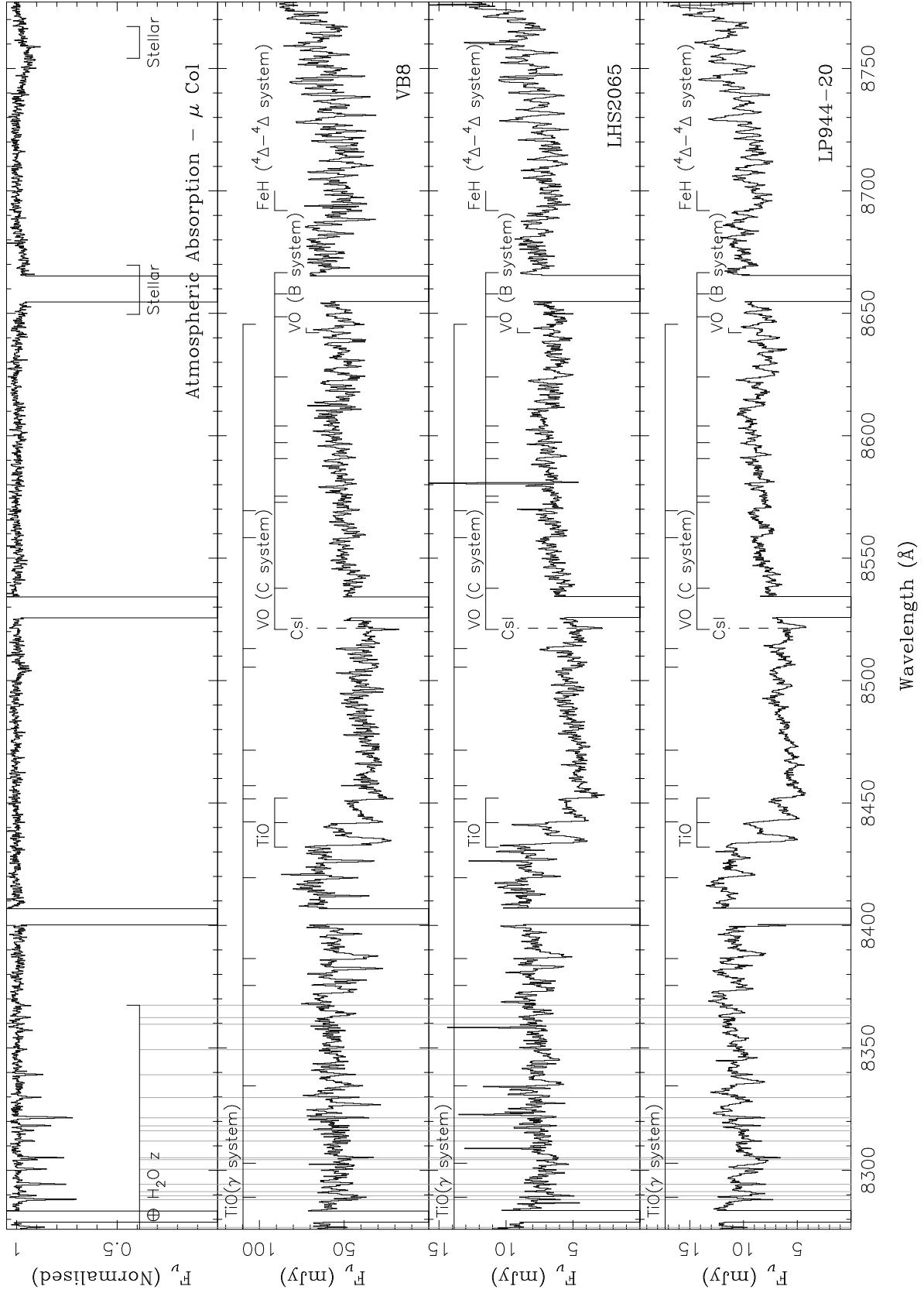


Figure 8. A spectral atlas for the objects VB8, LHS2065, and LP944-20 at 0.43\AA resolution (continued).

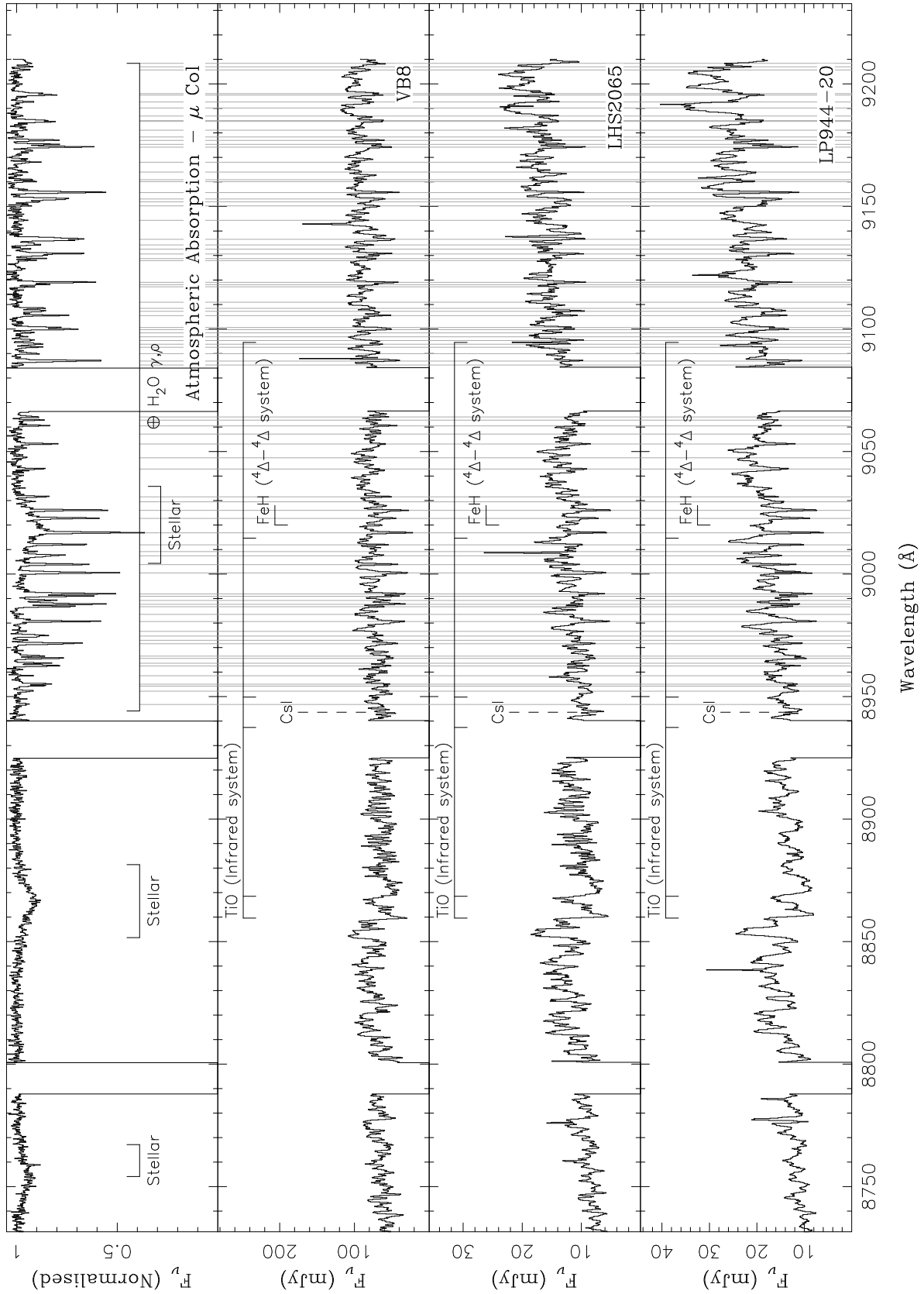


Figure 9. A spectral atlas for the objects VB8, LHS2065, and LP944-20 at 0.43Å resolution (continued).

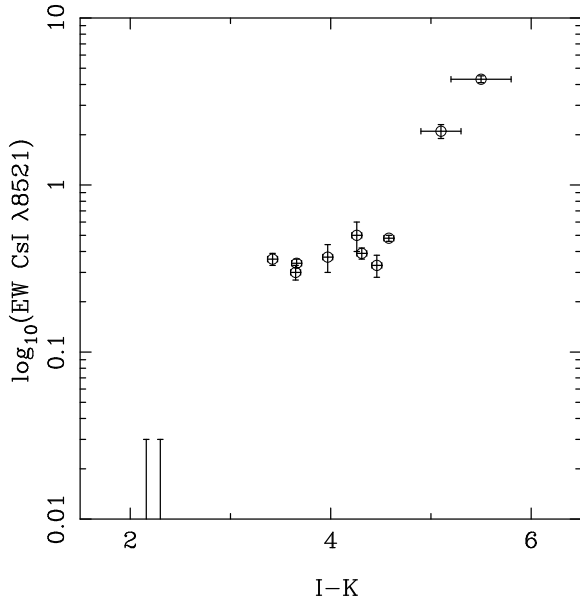
Table 7. Cs I and Rb I Observations

Object	I-K	Pseudo-Equivalent Widths (Å)		
		Rb I 7800Å	Rb I 7948Å	Cs I 8521Å
LP 944-20	4.58	0.87±0.05	0.73±0.05	0.48±0.02
BRI 1222-1222	4.31	0.88±0.03	0.83±0.05	0.39±0.03
ESO 207-61	4.18	0.94±0.06	1.03±0.14	^a
LHS 2065	4.46	0.81±0.03	0.62±0.05	0.33±0.05
LHS 2351	3.65	0.76±0.05	0.63±0.05	0.30±0.03
LHS 2397a	4.26	0.87±0.02	0.96±0.05	0.50±0.10
LHS 2875	2.05	0.16±0.02	-	-
LHS 2876	3.59	1.20±0.20	1.20±0.10	-
LHS 3003	3.66	0.84±0.02	0.86±0.03	0.34±0.02
LHS 427	2.30	0.23±0.01	0.17±0.01	<0.03
LHS 428	2.16	0.19±0.01	-	<0.03
LHS 429	3.42	1.02±0.02	0.95±0.03	0.36±0.03
LHS 474	3.97	0.93±0.05	0.93±0.05	0.37±0.07
DENIS-P J1058 ^b	5.1	-	-	2.1
DENIS-P J1228 ^b	5.5	-	-	4.3

NOTES:

a – Cs I 8521Å was detected in ESO 207-61, but could not be measured because its apparent radial velocity moved the Cs I 8521Å line onto the end of an echelle order.

b – I-K from Delfosse et al. 1997. Equivalent widths for Cs I from Martín et al. 1997. M_{bol} estimates from Delfosse et al. 1997.


Figure 11. Strength of Cs I lines as a function of I-K colour for the objects in Table 7.

Cs I line strengths are plotted in Figure 11. The observations describe a plateau at $EW=0.2-0.3\text{Å}$ throughout the late M-dwarf range, with considerably weaker absorption for the early M-dwarfs (as represented by the two upper limits), and considerably stronger absorption for objects below $\sim 2000\text{K}$. This diagram highlights the possible utility of the Cs I 8521Å line as a low-resolution spectroscopic indicator of effective temperature – at least for the purpose of discriminating extremely cool objects like DENIS-P J1228 and DENIS-P J1058 (for which it has been proposed that an entirely new spectral type (“L”) is required; Kirkpatrick 1998) from late-type M dwarfs.

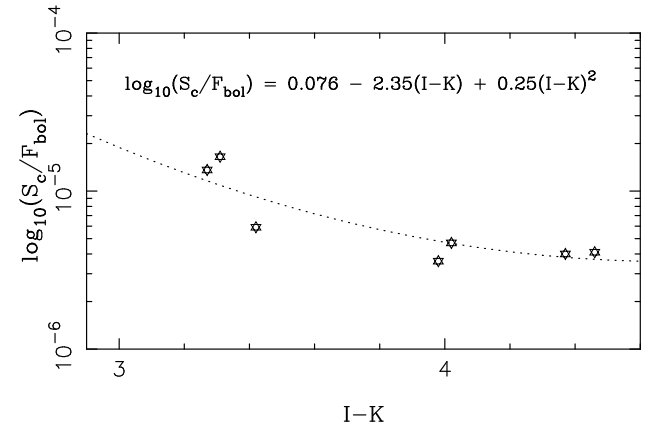
Table 8. CASPEC H α Emission Measurements

Object	UT	H α EW ^a (Å)	$[L_{H\alpha}/L_{bol}]^b$
BRI 0021-0214	1993/6/28 07:55:22	<2	< -5.1
LP 944-20	1993/6/28 09:53:58	<2	< -5.1
	1994/2/09 01:15:52	0.6±0.2:	-5.6
BRI 1222-1222	1994/2/08 09:00:17	4.7±0.5	-4.7
ESO 207-61	1994/2/08 02:17:06	2.8±0.5	-4.9
	1994/2/09 03:04:46	2.6±0.8:	-5.0
LHS 2065	1994/2/08 04:22:29	24.9±0.3	-4.0
LHS 2351	1994/2/09 05:44:56	6.1±0.1	-4.3
LHS 2397a	1994/2/08 06:13:18	47.3±0.8	-3.7
	1994/2/09 06:59:29	34.6±1.0	-3.9
LHS 2875	1994/2/09 07:59:21	0.20±0.02a	
LHS 2876	1994/2/09 08:40:30	1.6±0.5	-4.9
LHS 3003	1994/2/09 07:35:41	4.1±0.3	-4.6
LHS 427	1994/2/08 09:37:38	0.24±0.01a	
LHS 428	1993/6/28 03:04:22	1.8±0.4	-3.5
	1994/2/08 09:42:51	1.6±0.1	-3.6
LHS 429	1993/6/28 02:17:11	20.4±1.3	-3.7
	1994/2/08 09:25:37	3.7±0.2	-4.5
	1994/2/09 09:31:43	4.1±0.1	-4.4
LHS 474	1993/6/28 03:32:50	4.4±0.7	-4.7

NOTES:

a – “<” indicates a 3- σ upper limit. “:” indicates a marginal detection. “a” indicates the line was detected in absorption. Other results are actual measurements.

b – Upper limits are indicated by <. Measurements have an uncertainty of ± 0.2 largely due to the calibration from equivalent width to $[L_{H\alpha}/L_{bol}]$.


Figure 12. H α “bolometric correction” as a function of I-K colour for VLM stars from Tinney, Mould & Reid 1993. Also shown is the calibration relation adopted to derive the $[L_{H\alpha}/L_{bol}]$ values derived in Table 8

5.2 H α Emission

H α emission is seen in low mass stars when magnetic fields heating the outer atmosphere producing temperatures of up to $\sim 10^6$ K in the outer corona. Closer to the photosphere the chromosphere shows lower temperatures of $\lesssim 10^4$ K, where resonance lines of Ca II and Mg II, and the hydrogen Balmer lines are produced (HGR). H α emission equivalent widths for our Palomar observations were reported in RTM. Table 8 lists similar measurements for our ESO program objects, including only those observations yielding either detections

or significant upper limits. Because of poor seeing during our 1993 July observations, these come mostly from 1994 February.

Equivalent width (EW) is a measure of line flux ($F_{H\alpha}$), measured relative to the local continuum flux density (S_c).

$$EW \approx \frac{F_{H\alpha}}{S_c}$$

A large equivalent width does not necessarily imply strong chromospheric activity. A better indicator is the ratio of the luminosity in the $H\alpha$ line to the total bolometric luminosity of the star, $L_{H\alpha}/L_{bol}$, or its common logarithm ($[L_{H\alpha}/L_{bol}]$). Since our observations were not made with a spectrophotometric wide slit, line fluxes could not be measured directly. However, the EW can be converted to $L_{H\alpha}/L_{bol}$ if the ratio of the local continuum flux density S_c to the bolometric flux (F_{bol}) is known. Since,

$$\frac{L_{H\alpha}}{L_{bol}} = \frac{F_{H\alpha}}{F_{bol}} = \frac{EW \cdot S_c}{F_{bol}}$$

The ratio S_c/F_{bol} is just a bolometric correction. We can therefore derive a functional form for it, dependent on effective temperature or bolometric luminosity. We have calculated this quantity for the sample of objects with calibrated optical spectra and bolometric fluxes given in Tinney, Mould & Reid (1993), and the results are shown in Fig 12. The mean calibration was then used to derive the $[L_{H\alpha}/L_{bol}]$ estimates shown in Table 8, with an estimated uncertainty of $\approx \pm 0.2$. Full discussion of these results is deferred to §7.

6 ROTATION

Estimates of the rotational broadening of our CASPEC target stars have been obtained by cross-correlating the target spectra against a template (*cf.* Tonry & Davis, 1979). The dispersion[†] of the cross correlation peak (μ) is then the quadratic sum of the dispersion of the instrumental broadening in each spectrum (τ – assumed the same in both), any intrinsic broadening in the template spectrum (σ_0) and the rotational broadening of the target spectrum (σ). Uncertainties in the measurement of μ render it impossible to measure values of $\sigma < \sqrt{2\tau^2 + \sigma_0^2}$. In the case of our CASPEC observations, $\tau = 6.8$ km/s, setting a detection limit for rotational broadening ($v \sin i$) of 9.6 km/s. The Palomar data have a FWHM resolution of 75 km/s and set no useful limits on stellar rotation.

Following Tonry & Davis we estimate the width w of the cross-correlation peak μ by fitting a parabola. However, unlike Tonry & Davis we have not sought to calibrate the relationship between this parabola width w and the Gaussian dispersion μ . Rather we derive an empirical calibration between w and $v \sin i$ by cross-correlating “spun-up” spectra of VB 8 against an independent observation of the same star. The rotationally-broadened spectra are constructed using the profiles given by Gray (1992, equation 17.12, $\epsilon = 0.5$),

[†] In this section we use the term “dispersion” to describe the quantity σ in the usual Gaussian parameterisation $f(x) \propto e^{-(x/\sigma)^2}$, which is related to the full width at half maximum (FWHM) by $\sigma \approx \text{FWHM}/2.354$.

Table 9. CASPEC Rotational Measurements

Object	UT	$v \sin i^a$ (km/s)
BRI0021-0214	28 Jul 1993 07:55:22	42.5±8.4
	29 Jul 1993 08:36:41	40.1±8.6
LP 944-20/BRI 0337-3535 ^b	28 Jul 1993 09:53:58	28.3±1.9
	29 Jul 1993 10:17:28	28.4±3.9
	09 Feb 1994 01:15:52	28.1±1.8
BRI 1222-1222	08 Feb 1994 09:00:17	<17
	BR 2339-0447 ^d	<22
ESO 207-61	08 Feb 1994 02:17:06	<18
	09 Feb 1994 03:04:46	<19
LHS 234/G1 283B	09 Feb 1994 04:25:04	<14
LHS 2065	08 Feb 1994 04:22:29	<18
LHS 2351	09 Feb 1994 05:44:56	<16
LHS 2397a	08 Feb 1994 06:13:18	23.1±3.2 ^b
	09 Feb 1994 06:59:29	23.6±1.8 ^b
LHS 2875	29 Jul 1993 23:42:57	<22
	09 Feb 1994 07:59:21	<17
LHS 2876	09 Feb 1994 08:40:30	<18
LHS 3003	09 Feb 1994 07:35:41	<13
LHS 427/G1 643	28 Jul 1993 02:50:07	<19
	08 Feb 1994 09:37:38	<18
LHS 428/G1 644AB	28 Jul 1993 03:04:22	30.5±3.6 ^c
	08 Feb 1994 09:42:51	<19
LHS 474/G1 752B/VB 10	28 Jul 1993 03:32:50	<19
	29 Jul 1993 04:25:38	<19
LHS 511/G1 831	28 Jul 1993 05:47:10	<19

NOTES:

a – < indicates a 3- σ upper limit calculated as described in the text. Other results are actual measurements.

b – The velocities shown are only marginally above the 3- σ detection threshold for these observations.

c – Evidence was seen in the cross-correlation function for a double peak. This system is multiple so the width measured is probably due to orbital motion, not rotation.

d – An M7-8III giant (Kirkpatrick, Henry & Irwin 1997).

computed for a series of velocities between 0 and 50 km/s. The resulting w -to- $v \sin i$ calibration was calculated independently for each order.

Our calibration assumes that VB 8, the template for our VLM sample, has negligible rotation and there are no previous observational constraints of this parameter. As a test, we have repeated our w - $v \sin i$ calibration procedure using G1 643, which has a measured rotational upper limit of $v \sin i < 2.7$ km/s (Delfosse et al, 1998), cross-correlating against the VB 8 template. The resulting relation is essentially identical to that derived using VB 8 alone, implying that the latter star has a rotation substantially lower than our instrumental resolution of $\tau = 6.8$ km/s.

The rotational velocity for each target star was then estimated as follows: each order was cross-correlated with the appropriate template star order; the width w of the highest peak in the cross-correlation was measured, if its confidence level exceeded 90% (Tonry & Davis, equation 33); the uncertainty in the measurement of this width Δw was also estimated (Tonry & Davis, equation 25); if the measured width was less than $w_0 + 3\Delta w$, then this measurement is treated as an upper limit at the $v \sin i$ corresponding to $w = w_0 + 3\Delta w$, otherwise the measured width was treated as a velocity measurement at the appropriate $v \sin i$; and lastly, the resulting rotation measures were averaged over the available orders.

The results of this process are shown in Table 9. Typical uncertainties in Δw range from 0.2 km/s for bright stars to 2 km/s for faint ones. This results in $3\text{-}\sigma$ rotation detection thresholds ranging from 15 to 22 km/s. In other words, given the resolution of our observations, we are only sensitive to very fast rotators. Significant rotation was detected in only two objects: BRI 0021-0214 and LP 944-20. LHS 2397a seems to show possible evidence for rotation right at the detection limit for this star of ≈ 23 km/s. Gl 644AB showed some evidence for broadening in 1993 July, but none in 1994 February. Given the multiple nature of this system, and evidence seen for a double peak in the cross correlation function, it seems reasonable to assume that the broadening observed in 1993 is more likely due to orbital motions than stellar rotation. The effect of rapid rotation can be seen in the spectra for LP 944-20 plotted in Figures 4-9, where both atomic and molecular features are noticeably broader than those observed in LHS 2065 or VB 10. Of the two stars in which we detect rotation, only BRI 0021-0214 has been previously measured. The value of 41 ± 8 km/s we measure for BRI 0021-0214 compares favourably with the 40 ± 7 km/s measured by Basri & Marcy (1995).

7 ROTATION & ACTIVITY

The standard picture of the chromospheric activity (as revealed by $H\alpha$ emission) is that it is a product of stellar magnetic fields, via the effects of stellar rotation and convection combining to form a dynamo. In this picture, the activity is related directly to stellar rotation. Such a model is now well established for F,G and K-type stars (Hartmann & Noyes 1987). Stellar rotation rate is also a function of age – the rotation of a star slows as it loses angular momentum and “spins down”. The spin down rate is generally held to be a function of mass, with lower mass stars spinning down more slowly (eg. Stauffer et al. 1994).

As a result a general relationship between chromospheric activity and age can be deduced, at least for F, G and K dwarfs, though this relationship is complicated by the fact that stars are born with an initial spread in angular momentum, producing considerable scatter about the overall relationship between chromospheric activity and age. This is evidenced by the large spread seen in the rotational velocities of stars in young and intermediate-age clusters: for example, G dwarfs in the Pleiades (≈ 100 Myr) have $v \sin i < 6 - 50$ km/s, while M dwarfs in the Hyades (≈ 600 Myr) show $v \sin i < 10 - 20$ km/s (Stauffer et al. 1994).

The situation for low mass M dwarfs, however, is less clear. The appearance of $H\alpha$ emission increases with spectral type from M0 ($\approx 10\%$) to M6 ($\approx 50\%$). It has been suggested that this is because $H\alpha$ becomes easier to detect as the continuum flux at 6562\AA decreases. However, the ratio of the $H\alpha$ luminosity to the bolometric luminosity ($L_{H\alpha}/L_{bol}$) spans an approximately constant range of activity at $[L_{H\alpha}/L_{bol}] = -3.5$ to -4.2 (HGR), rather than declining with decreasing luminosity, as one would expect if a selection effect were responsible for the higher dMe fraction.

The straightforward interpretation of this result is that the proportion of rapidly rotating M-dwarfs increases with spectral type. Delfosse et al. (1998) have studied the rotation of a sample of M-dwarfs, and find the expected correla-

tion with rotation – all stars with $v \sin i > 15$ km/s show chromospheric activity at the $[L_{H\alpha}/L_{bol}] = -3.5$ to -4 level, while stars with no significant rotation detected show $\log_{10}[L_{H\alpha}/L_{bol}] = -4$ to -4.5 . Thus, this result suggests that the higher fraction of late-type dMe dwarfs may reflect longer spin-down times at very low masses.

However, the fast rotators detected in our CASPEC study throw a spanner into this neat picture. Basri & Marcy (1995) first pointed out that BRI 0021-0214 is extremely late in spectral type ($> M9.5V$, Kirkpatrick et al. 1997), and a fast rotator, *but* shows no $H\alpha$ in emission. Since then Tinney et al. (1997) have found BRI 0021-0214 to emit $H\alpha$ at very weak levels ($1.30 \pm 0.05\text{\AA}$ EW). This corresponds to only $[L_{H\alpha}/L_{bol}] = -5.3$ (cf. §5.2) making this to all intents and purposes a chromospherically inactive star, and directly contradicting the generally held activity-rotation connection.

LP 944-20, with $[L_{H\alpha}/L_{bol}] \approx -5.6$ and $v \sin i = 28$ km/s, represents the detection of a second member of this class of “inactive, rapidly rotating” objects. Moreover, in this case we can add the further physical parameters that the inactive, rapid rotator is a brown dwarf of mass $0.06 M_{\odot}$, and age 475-650 Myr (Tinney 1998). The recently discovered brown dwarf DENIS-P J1228.2-1547 ($v \sin i = 20$ km/s, $[L_{H\alpha}/L_{bol}] \approx -5.3$), and the brown dwarf candidate DENIS-P 1058.7-1548 (23 km/s, ≈ -5.4) also fall into this group (Martín et al. 1997; Tinney et al. 1997). These objects may represent an entire class of objects at or below the hydrogen burning main sequence which show substantially reduced levels of chromospheric activity, despite the presence of levels of stellar rotations which would produce significant activity in an M0-6 dwarf.

Is this violation of the rotation-activity connection purely a function of mass? Observations of nearby clusters suggest that this may be the case. Activity (as measured by $[L_{H\alpha}/L_{bol}]$) amongst Pleiades M-dwarfs rises monotonically with decreasing luminosity (and mass) until $M_{bol} \approx 10$, at which point the relative flux in $H\alpha$ drops sharply. Figure 6(b), for example, of Reid, Hawley & Mateo (1995) shows that for luminosities below $M_{bol} \approx 10$, $[L_{H\alpha}/L_{bol}]$ falls from ≈ -3.5 to ≈ -4.5 . Similar results have been derived by Stauffer et al. (1994), Hodgkin, Jameson & Steele (1995) and Oppenheimer et al. (1997), while Reid & Hawley (1998) have detected comparable behaviour amongst Hyades stars.

Spectroscopy of Pleiades brown dwarfs shows that similar mass objects to LP944-20 and DENIS-P J1228 (Rebolo, Zapatero Osorio, Martín 1995; Basri, Marcy & Graham 1996; Zapatero Osorio et al. 1997) have $H\alpha$ lines with equivalent widths of $\sim 5 - 10\text{\AA}$, which corresponds to $[L_{H\alpha}/L_{bol}] \approx -4.5$ to -4.8 (§5.2) at age $\sim 70 - 120$ Myr.

We therefore conclude that (1) we see evidence in the Pleiades for a trend towards lower chromospheric activity at masses below $\approx 0.1 M_{\odot}$, and (2) that we see no evidence for a significant change in this trend as the brown dwarf limit is crossed. Moreover, the Pleiades VLM stars studied by Oppenheimer et al. (1997) are all rapid rotators, with $v \sin i$ in the range 37–65 km/s. This implies that Pleiades age objects just above the H-burning limit already violate the rotation-activity connection. The “inactive rapid-rotators” detected in the field continue this violation below the H-burning limit. Age does not seem to play a *determining* role, since both $\sim 70 - 100$ Myr VLM stars and $\sim 500 - 1000$ Myr brown dwarfs are found to rotate rapidly, and yet to be

substantially inactive. However, there is evidence for a decrease in activity as VLM stars and brown dwarfs age, since $[L_{H\alpha}/L_{bol}]$ falls from ~ -4.5 – -4.8 to ~ -5.1 – -5.3 as we move from Pleiades age brown dwarfs to ~ 500 – 1000 Myr brown dwarfs like LP 944-20 and DENIS-P J1228.2-1547.

It should be noted however, that the possible identification of decreasing mass as a parameter well correlated with the violation of the rotation-activity connection, does not necessarily imply that mass is the controlling physical parameter. The absence of chromospheric activity implies either the absence of magnetic fields, or the suppression of the chromospheric heating mechanism. In either case this could be physically due to luminosity or effective temperature dependent effects (eg. the formation of dust which begins at VLM effective temperatures), as well as to the internal structure imposed on these objects by their mass.

Confirmation of the rapid rotation of these objects via the search for periodic modulation needs to be made a high priority. Many very low-mass stars show periodic modulations due to star spots. Even if the inactive, rapid rotators have no spots, they may exhibit periodic variation due to the transit across their disk of dust clouds. In either case (spots or clouds) the result will be the passage of regions of apparently low effective temperature across their disk. Such regions should show a clear signature in the regions of the spectrum where TiO absorption is strong in late M-dwarfs, but absent in cooler objects like DENIS-P J1228 (Tinney et al. 1997).

The inactive, rapid rotators represent a direct counter-example to the generally held picture of the activity-rotation connection. Unravelling of this mystery will provide valuable insights into both the interiors of brown dwarfs, and the mechanics of magnetic field and chromosphere generation.

8 CONCLUSION

We have obtained high resolution optical spectroscopy of a sample of VLM stars and one brown dwarf. Analysis of the kinematics of these stars show no evidence for a significant kinematic difference between either our photometrically-selected or proper-motion-selected sample, and a sample of more massive nearby M-dwarfs.

We present 0.43\AA resolution observations of two VLM stars and one intermediate age brown dwarf, for use as a spectroscopic atlas, together with identifications for their major stellar atomic and molecular features. Pseudo-equivalent widths for the Cs I and Rb I features present in these are obtained. The Cs I 8521\AA feature in particular shows promise for discriminating L-type from M-type dwarfs in low resolution spectra.

Measurements of the $H\alpha$ emission equivalent widths and stellar rotations are presented. These reveal that the brown dwarf LP 944-20 is an “inactive, rapid rotator”, like the M-dwarf BRI 0021-0214 and the VLM Pleiades objects of Oppenheimer et al. (1997). This discovery shows that violation of the rotation-activity connection continues below the bottom of the H-burning main sequence. The fact that such violation occurs for both Pleiades-age VLMs and for a ~ 500 Myr old brown dwarf, indicates that age is not the determining factor in such a violation.

Acknowledgments

We would like to thank the technical and astronomical support staff at the ESO La Silla and Palomar Observatory for their most professional assistance throughout this observing program. The authors would like to thank X.Delfosse for communicating the results of OHP observations prior to publication, and J.Mould for helpful discussion.

REFERENCES

- Allen, C.W. 1976, *Astrophysical Quantities*, Athlone Press: London
- Basri, G. & Marcy, G.W. 1995, *AJ*, 109, 762
- Basri, G., Marcy, G.W. & Graham, 1996, *ApJ*, 458, 600
- Delfosse, X. et al. 1997, *A&A*, 327, L25
- Delfosse, X., Forveille, T., Perrier, C. & Mayor, M. 1998, *A&A*, 331, 581
- Gatterer, A., Junkes, J. & Salpeter, E.W. 1957, *Molecular Spectra of Metallic Oxides*, Specola Vaticana: Vatican City.
- Gliese, W. & Jahreiss, H. 1991, *Catalogue of Nearby Stars III*, in *The Astronomical Data Center CD-ROM: Selected Astronomical Catalogs*, Vol. 3, L.E. Brodzmann and S.E. Gesser (eds), NASA/ADC, Greenbelt, MD, USA
- Gray, D.F. 1992, *The observations and analysis of stellar photospheres*, 2nd Edn, Cambridge University Press: Cambridge
- Gullixson, C.A., Boeshaar, P.C., Tyson, J.A. & Seitzer, P. 1995, *ApJS*, 99, 281
- Harrington, R.S. et al. 1993, *AJ*, 105, 1571
- Hartmann, L.W. & Noyes, R.W. 1987, *ARAA*, 25, 271
- Hawkins, M.R.S. & Bessell, M.S. 1988, *MNRAS*, 234, 177
- Hawley, S.L., Gizis, J.E., & Reid, I.N. 1995, *AJ*, 113, 1458 (HGR)
- Henry, T.J. & McCarthy Jr, D.W. 1990, *ApJ*, 350, 334
- Henry, T.J. & McCarthy Jr, D.W. 1993, *AJ*, 106, 773
- Hodgkin, S.T., Jameson, R.F. & Steele, I.A. 1995, *MNRAS*, 274, 869
- Kirkpatrick, J.D. 1998 in “Brown Dwarfs and Extra-solar Planets”, A.S.P. Conference Series, eds. Rebolo, R., Martín, E. & Zapatero Osorio, M., p.405
- Kirkpatrick, J.D., Henry, T.A. & Irwin, M.J. 1997, *AJ*, 113, 1421
- Kirkpatrick, J.D., Henry, T.A. & McCarthy Jr., D.W. 1991, *ApJS*, 77, 417
- Kirkpatrick, J.D. & McCarthy Jr., D.W. 1994, *AJ*, 107, 333
- Kirkpatrick, J.D., McGraw, J.T., Hess, T.R., Liebert, J. & McCarthy Jr., D.W. 1994, *ApJ*, 94, 749
- Leggett, S.K. 1992, *ApJS*, 82, 351
- Leinert, Ch., Haas, M., Allard, F., Wehrse, R., McCarthy Jr, D.W., Jahreiss, H. & Perrier, Ch. 1990, *A&A*, 236, 399
- Leinert, Ch., Henry, T., Glindenmann, A. & McCarthy Jr., D.W. 1997, *A&A*, 325, 159
- Luyten, W.J. 1979, *LHS Catalogue*, University of Minnesota: Minneapolis
- Marcy, G.W. & Benitz, K. 1989, *ApJ*, 344, 441
- Martín, E.L., Basri, G., Delfosse, X. & Forveille, T. 1997, *A&A*, 327, L29
- Monet, D.G., Dahn, C.C., Vrba, F.J., Harris, H.C., Pier, J.R., Luginbuhl, C.B. & Ables, H.D. 1992, *AJ*, 103, 638
- Mihalas, D. & Binney, J. 1981, *Galactic Astronomy*, p398. W. H. Freeman & Co.: San Francisco
- Oppenheimer, B., R., Basri, G., Nakajima, T. & Kulkarni, S.R. *AJ*, 113, 296
- Pearse, R.W.B. & Gaydon, A.G. 1976, *Identification of Molecular Spectra*, 4th edition, Wiley & Sons: New York
- Press, W.H., Flannery, B.P., Teukolsky, S.A. & Vetterling, W.T. 1986, *Numerical Recipes*, p472, Cambridge University Press: Cambridge
- Phillips, J.G. 1950, *ApJ*, 111, 314

- Phillips, J.G., Davis, S.P., Lindgren, B. & Balfour, W.J. 1950, *ApJS*, 65, 721
- Rebolo R., Zapatero Osorio M.R. & Martín E.L. 1995, *Nature* 377, 129.
- Reid, I.N. & Hawley, S.L. 1998, in preparation
- Reid, I.N., Hawley, S.L. & Gizis, J.E. 1995, *AJ*, 110, 1838
- Reid, I.N., Hawley, S.L. & Mateo, M. 1995, *MNRAS*, 272, 828
- Reid, I.N. & Gilmore, G. 1984, *MNRAS*, 206, 19
- Reid, I.N. & Gizis, J.E. 1997, *AJ*, 113, 2246
- Reid, I.N., Tinney, C.G. & Mould, J.R. 1994, *AJ*, 108, 1456 (RTM)
- Schweitzer, A., Hauschildt, P.H., Allard, F. & Basri, G. 1996, *MNRAS* 283, 821
- Solf, J. 1978, *A&AS*, 34, 409
- Stauffer, J.R., Leibert, J., Giampapa, M., Macintosh, B., Reid, N. & Hamilton, D. 1994, *AJ*, 108, 160
- Tinney, C.G. 1993, *ApJ*, 414, 279
- Tinney, C.G. 1996, *MNRAS*, 281, 644
- Tinney, C.G. 1997, in "Brown Dwarfs and Extra-solar Planets", A.S.P. Conference Series, eds. Rebolo, R., Martín, E. & Zapatero Osorio, M., p.75
- Tinney, C.G. 1998, *MNRAS*, 296, L42
- Tinney, C.G., Delfosse, X. & Forveille, T., 1997, *ApJ*, 490, L95
- Tinney, C.G., Mould, J.R. & Reid, I.N. 1993, *AJ*, 105, 1045
- Tinney, C.G., Reid, I.N., Gizis, J. & Mould, J.R. 1995, *AJ*, 110 3014
- Tonry, J. & Davis, M. 1979, *AJ*, 84, 1511
- Turnshek, D.A., Bohlin, R.C., Williamson, R.L., Lupie, O.L. & Koorneef, J., 1990, *AJ*, 99, 1243
- Turnshek, D.E., Turnshek, D.A., Craine, E.R. & Boeshaar, P.C. 1985, *An Atlas of Digital Spectra of Cool Stars*, Western Research Co.: Tucson
- van Altena W.F., Lee J.T. & Hoffleit E.D. 1995, *General Catalogue of Trigonometric Stellar Parallaxes, Fourth Edition*, in *The Astronomical Data Center CD-ROM: Selected Astronomical Catalogs, Vol. 3*, L.E. Brodzmann and S.E. Gesser (eds), NASA/ADC, Greenbelt, MD, USA
- Weis, E.W. 1988, *AJ*, 96, 1710
- Zapatero Osorio, M. R., Rebolo, R., Martín, E. L., Basri, G., Magazzu, A., Hodgkin, S. T., Jameson, R. F. & Cossburn, M. R. 1997, *ApJ*, 491, L81